DOI: 10.1111/j.1467-8659.2010.01846.x

COMPUTER GRAPHICS *forum*
Volume 30 (2011), number 6 pp. 1603–1616

Adaptive Records for Irradiance Caching

Mickaël Ribardière[1,2], Samuel Carré[1] and Kadi Bouatouch[3]

[1]Centre Scientifique et Technique du Bâtiment (CSTB), France
mickael.ribardiere@irisa.fr
[2]Université de Rennes 1, France
samuel.carre@cstb.fr
[3]IRISA - INRIA Rennes, France
kadi.bouatouch@irisa.fr

Abstract

Irradiance Caching is one of the most widely used algorithms to speed up global illumination. In this paper, we propose an algorithm based on the Irradiance Caching scheme that allows us (1) to adjust the density of cached records according to illumination changes and (2) to efficiently render the high-frequency illumination changes. To achieve this, a new record footprint is presented. Although the original method uses records having circular footprints depending only on geometrical features, our record footprints have a more complex shape which accounts for both geometry and irradiance variations. Irradiance values are computed using a classical Monte Carlo ray tracing method that simplifies the determination of nearby objects and the pre-computation of the shape of the influence zone of the current record. By gathering irradiance due to all the incident rays, illumination changes are evaluated to adjust the footprint's records. As a consequence, the record footprints are smaller where illumination gradients are high. With this technique, the record density depends on the irradiance variations. Strong variations of irradiance (due to direct contributions for example) can be handled and evaluated accurately. Caching direct illumination is of high importance, especially in the case of scenes having many light sources with complex geometry as well as surfaces exposed to daylight. Recomputing direct illumination for the whole image can be very time-consuming, especially for walkthrough animation rendering or for high-resolution pictures. Storing such contributions in the irradiance cache seems to be an appropriate solution to accelerate the final rendering pass.

Keywords: rendering, global illumination, irradiance cache

ACM CCS: I.3.7 [Computer Graphics]: Three-Dimensional Graphics and Realism

1. Introduction

Computing global illumination in a reasonable time still is a challenge in computer graphics. To take up this challenge, Irradiance/Radiance caching is one of the most widely used algorithms [WRC88, WH92, TL04, KBPv06, KGW*08]. The original Irradiance caching [WRC88] is a ray tracing-based method that computes the indirect diffuse illumination component. It relies on the fact that indirect irradiance changes slowly over the object surfaces. Indirect illumination is computed for a sparse set of points, called records, and stored in a cache. Direct illumination is evaluated using classical techniques (shadow map for point light sources, Monte Carlo ray tracing for area light sources for example), whereas indirect illumination is computed either by a Monte Carlo method for the records or using interpolation for the other points.

In some applications, direct illumination can be very costly, for instance in architectural design or in lighting projects requiring accurate and physically based results (spectral quantities with many wavelets, not only three as usual). The scene may have many area light sources of complex geometry and specific photometric characteristics. Daylight (sun and sky) is often present as well. In such cases,

direct illumination computation can be very time demanding. When using Ward's irradiance caching method, caching the indirect and the direct irradiances would yield low-quality results. Indeed, direct illumination changes quickly over surfaces because of occlusions (shadows). The original Irradiance Caching method [WRC88] and the original gradients [WH92] cannot compensate for high illumination changes because the record density must be proportional to the rate of illumination change. In addition, gradients are used for computing smooth changes over surfaces and cannot detect occlusions in case of translation. Furthermore, the record density is only controlled by geometry and not by illumination results. This is not sufficient in complex indirect illumination cases in which a significant indirect illumination source illuminates the scene and produces shadows.

This paper presents an adaptive Irradiance Caching algorithm, which adapts the record density depending on the surface geometry and the illumination changes. This density control reduces the number of cached records along edges and corners. The record density has to be proportional to the change rate of direct and indirect illumination when high gradients are detected. A novel gradient is proposed to detect these significant illumination changes to adaptively determine the shape and size of the record footprints. This method straightforwardly includes both direct and indirect illumination in the same cache. It is then efficient in terms of direct illumination from complex light sources. Furthermore, storing all kinds of illumination in records allows to easily reuse the cache for interpolation of global illumination at points different from records.

The paper is organized as follows: Section 2 summarizes the related works, whereas a background is presented in Section 3 for a clear presentation of our method in the rest of the paper. Then Section 4 describes adaptive record footprints. Section 5 explains how gradients including direct illumination are computed. Section 6 shows how to adapt the size of the influence zone of a record depending on the interpolation accuracy needed. Finally, Section 7 presents and discusses some results before concluding.

2. Related Work

The technique proposed in this paper is based on the classical Irradiance Caching algorithm. Irradiance Caching was introduced by Ward *et al.* [WRC88] to speed up global illumination computations based on Monte Carlo ray tracing. It has been widely used ever since [KGW*08]. The algorithm takes advantage of spatial coherence of irradiance. Irradiance is computed for only a few points over the surfaces of the scene and then interpolated to reconstruct the radiance for each other point. In [WH92], Ward and Heckbert improved this interpolation scheme by using irradiance gradients. As said before, the original algorithm only caches irradiance due to indirect illumination.

In [SM02], Smyk *et al.* increased the density of records according to the gradient magnitude to better reconstruct high changes of indirect illumination. This density is controlled by modifying the records radii. However, this method adds a considerable number of records around the corners and the edges of the scene. Tabellion and Lamorlette [TL04] proposed several improvements of the original method such as using a minimum distance to the near objects instead of the harmonic mean to determine a record radius. As in [SM02], an excessive record density may be assigned to concave objects. In the same way, Křivánek *et al.* [KBPv06] (see [KGW*08] too) proposed other practical modifications to the original Ward *et al.*'s method to make it more practical. With *Adaptive Caching* the spatial density of the cached values gets variable. The change rate of indirect illumination controls this adaptive density to avoid visible interpolation artefacts. The overlapping area of a record which includes a discontinuity in the interpolation will then be reduced. If the change rate in indirect illumination is too high then the radius of a record is smaller, which increases the record density. Unfortunately, with this adaptive caching method, the record which provides the highest discontinuity is often the one which is closest to the considered point and which provides the best interpolation. Such records may be very important for a good interpolation and reducing its zone may add a lot of records in the cache. Imagine that we want to compute the irradiance at point P overlapped by three irradiance records called R_1, R_2 and R_3. If R_1 is much closely located to P than the other records, then R_1 is intuitively the record which should contribute the most to the irradiance interpolation in P. But applying the Křivánek's adaptive caching method in such context will remove the record R_1 from the computation of the irradiance at P, as R_1 is the record which causes the biggest discontinuity.

Křivánek *et al.* presented in the same paper [KBPv06] another improvement referred to as *neighbour clamping*. This technique minimizes the ray-leaking problem caused by a poor detection of nearby objects. The radius of a record is controlled as well as all its nearby records. Thus, there are more chances to detect small sources of indirect illumination.

As an extension to glossy surfaces, *Radiance Caching* has been proposed. It consists in projecting the incoming radiances stored in records into a spherical or hemispherical harmonics basis [Gre03, GKPB04]. The Radiance Caching scheme was first proposed in [Kŏŏ5, KGPB05] by Křivánek *et al.* Illumination of diffuse and glossy surfaces are stored in the cache and high-frequency BRDF and specular reflections are computed in an additional pass. In [KGBP05], the authors improved radiance gradient computations. The radiance caching scheme has known several improvements. Recently, Herzog *et al.* in [HMS09] used an (r)radiance caching algorithm using the *lightcuts* method, an adaptive and hierarchical instant-radiosity based algorithm [WFA*05, WABG06]. As in [KGPB05], incident radiances are projected into a hemispherical harmonics basis. An interesting feature in this work

is the two-level radiance caching: the first one for indirect irradiance and the second for direct irradiance computed in parallel. Two caches are maintained as well as two light trees. The two caches are tested whereas direct and indirect irradiance computations are performed individually. Another interesting aspect is the multipass adaptive caching proposal. It is an extension of Křivánek *et al.*'s adaptive caching method [KBPv06]. It consists in reducing the record footprints in one dimension resulting in an ellipsoidal footprint only. In this paper, we focus only on diffuse reflections, glossy reflections could be computed in a second pass.

Other techniques allow to interpolate direct and indirect illumination from sparse samples to achieve interactive rendering. One of these methods is the *Render Cache* [WDP99, WDG02]. Only few pixels of the image are computed using ray tracing or path tracing. The values of these pixels are stored in a cache and reused for the subsequent frames. The other pixels of the current frame are computed using interpolation/smoothing filters. The result is an estimate of the current image. The *Render Cache* can also be reused across frames in a walkthrough context by reprojecting shaded pixels according to the new viewpoint. Another technique is the *Edge-and-Point Rendering* proposed by Bala *et al.* [BWG03] and extended by [VALBW06]. It is based on the *Render Cache*. *Edge-and-Point Rendering* improves the rendering of high discontinuity regions such as silhouettes and shadow boundaries by using an *Edge-and-Point Image*, which stores the discontinuities. The goal of the above techniques are well suited for interactive rendering but not for a complete and physically based lighting simulation.

3. Background

The Irradiance Caching algorithm exploits spatial coherence by sparsely sampling and interpolating indirect irradiance. Each record R stores the following information:

(1) x_R, position of the record,
(2) $\vec{n_R}$, normal at x_R,
(3) $E(R)$, irradiance computed at x_R,
(4) d_R, harmonic mean distance ([WRC88, KBPv06]) or minimum distance ([TL04]) to objects visible from x_R.

Let $a \cdot d_R$ be the radius of the influence zone of record R, where a is a user-defined constant related to the maximum error. If the influence zone of a record R covers a given point p it is not necessary to compute an irradiance value at p from scratch, but from the already computed irradiance value of R. The contribution of a record R to a point p is weighted by w_R^{Ward} whose expression is

$$w_R^{\text{Ward}}(p) = \left(\frac{\|x_p - x_R\|}{d_R} + \sqrt{1 - \vec{n_p} \cdot \vec{n_R}} \right)^{-1}. \quad (1)$$

Let S be the set of records surrounding point p:

$$S = \left\{ R : w_R^{Ward}(p) > \frac{1}{a} \right\}. \quad (2)$$

If S is not empty, the irradiance at p can be estimated as

$$E(p) = \frac{\Sigma_{R \in S} E(R) w_R^{\text{Ward}}(p)}{\Sigma_{R \in S} w_R^{\text{Ward}}(p)}. \quad (3)$$

The original weighting function [w_R^{Ward} in Equation (1)] has some undesirable properties. This function is not continuous at the border of the influence zone of a record as it does not tend towards zero. As proposed in [KGW*08], we use a slightly modified function w_R:

$$w_R(p) = \left(\frac{\|x_p - x_R\|}{d_R} + \sqrt{1 - \vec{n_p} \cdot \vec{n_R}} \right)^{-1} - \frac{1}{a}. \quad (4)$$

A record covers p if $w_R(p) > 0$. Otherwise, a new irradiance record is computed and added to the cache and p becomes the record position. Gradients proposed in [WH92, KGBP05] are designed for improving interpolation. Irradiance at x can be expressed by

$$E(x) = \int_\Omega L(x, \overrightarrow{\omega})(\overrightarrow{n_x} \cdot \overrightarrow{\omega})\, \mathrm{d}\overrightarrow{\omega}. \quad (5)$$

In the Irradiance Caching method, this value is computed using Monte Carlo ray tracing with an uniform distribution:

$$E(x) = \frac{2\pi}{N} \sum_{i=1}^{N} L_i(x, \overrightarrow{\omega_i})(\overrightarrow{n_x} \cdot \overrightarrow{\omega_i}), \quad (6)$$

where N is the number of ray samples, L_i the incoming radiance for the ith sample in the direction $\overrightarrow{\omega_i}$ and $\overrightarrow{n_x}$ the normal at x. Consider $E_i(x) = 2\pi L_i(x, \overrightarrow{\omega_i})(\overrightarrow{n_x} \cdot \overrightarrow{\omega_i})$ as an estimate of the irradiance at x (up to a scaling factor 2π) due to the ith ray sample. In other words, it is an estimation of the irradiance due to the ith equivalent point source. The determination of equivalent point sources has been used in the *Bidirectional Path Tracing* method [VG94, Vea98, LW93] (Figure 1). An equivalent point light source corresponds to a point light or an eye path which is directly connected to x_R, the position of a new record R (x_R is the first vertex in eye path). Now we can substitute $L_i(x, \overrightarrow{\omega_i})(\overrightarrow{n_x} \cdot \overrightarrow{\omega_i})$ in Equation (6):

$$E(x) = \frac{1}{N} \sum_{i=1}^{N} E_i(x). \quad (7)$$

Knowing E_i and using ray tracing, an equivalent intensity $I_i^{\text{eq}}(\overrightarrow{\omega_i})$ characterizing the ith equivalent point light source can be expressed:

$$I_i^{\text{eq}}(\overrightarrow{\omega_i}) = \frac{E_i(x) \cdot d_i^2}{\overrightarrow{n_x} \cdot \overrightarrow{\omega_i}}, \quad (8)$$

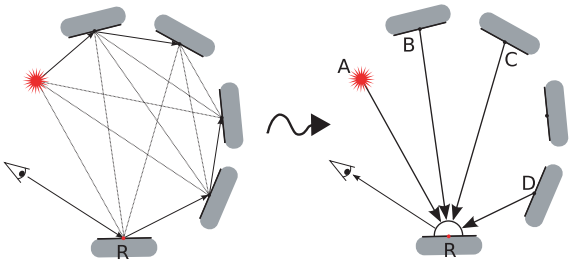

Figure 1: *A sample with Bidirectional Path Tracing: this sample allows us to know three indirect contributions (B , C and D) and one direct contribution (A) for R corresponding to four equivalent point sources. More tracing would give full coverage of the hemisphere above R.*

where d_i is the distance to the ith equivalent point source. For the new record R at position x, the irradiance becomes

$$E(x) = \frac{1}{N} \sum_{i=1}^{N} \frac{I_i^{eq}(\vec{\omega_i}) \cdot (\vec{n_x} \cdot \vec{\omega_i})}{d_i^2}. \quad (9)$$

Note that an equivalent light source will be considered as a secondary point light source located at the intersection point between a ray sample (generated from a point R) and the scene. The intensity of a equivalent point light source located at point R will be reused for another point R' close to R to evaluate the irradiance at point R' without tracing new sample rays as shown in Figure 6. This allows to significantly speed up our method. There are two types of equivalent point light source: direct if it lies on a primary light source, and indirect otherwise. As previously said, the original Irradiance Caching scheme does not store direct irradiance. Our method proposes improvements to this technique: use of a new shape of influence zone, a new gradient formulation, an adaptation to strong illumination changes, and the storage of both direct and indirect irradiances in the records. These contributions will be detailed later on.

4. Adaptive Records

Adapting the size of the influence zone of a record [KBPv06, HMS09] to the rate of illumination changes increases the number of records while providing better results. The cache density is then adapted to this rate of illumination changes. However, the number of records increases at the edges and the corners too regardless of the illumination changes. The same problem appears when using the minimum distance [TL04]. To avoid this problem, Tabellion and Lamorlette control the cache density by using the projected area of a pixel. This results in under-sampling far objects and adding a lot of records in case of animation rendering. Although it is necessary to increase the number of records to better estimate the rate of illumination changes, it is important not to increase the density where it is not necessary. We think that the over-sampling issue is due to the circular shape of the record's influence zones whose radii are defined by the minimum distance or the harmonic mean of distance to nearby objects. In this section, we propose a new record footprint which better adapts to the geometry. Figure 2 describes the main idea. To avoid shadow and light leaks, Tobler and Maierhofer [RFT06] proposed a similar idea to determine adaptive projection areas for density estimation in photon mapping.

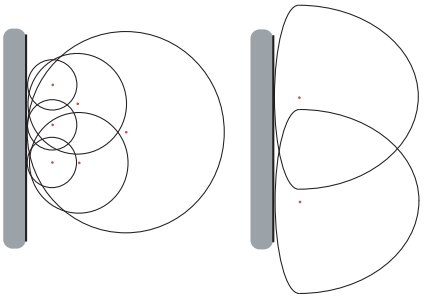

Figure 2: *With a circular influence zone of a record (left) more records are needed. With an influence zone that is small towards close objects and large towards far objects (right), a record covers a better shaped influence zone and finally less records are needed.*

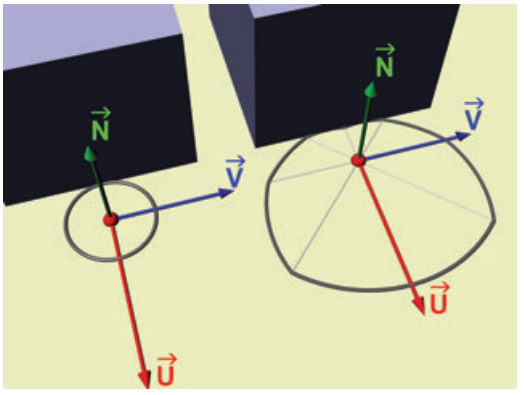

Figure 3: *Height pseudo-elliptic zones define the influence zone of a record (red balls). Here, the record is near a cube; a circular zone (on the left) is compared to an adaptive record zone (on the right).*

The ideal influence zone of a record can be represented by a planar surface with a curved boundary. This surface cannot be computed exactly but it is approximated through a discretization scheme as explained hereafter. This planar surface lies on the tangent plane associated with a record position and is described by an angular decomposition in height pseudo-elliptic zones as seen in Figure 3 . The local

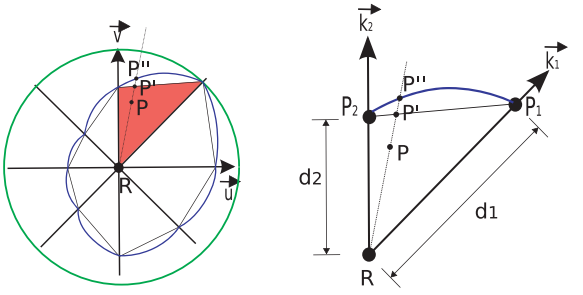

Figure 4: *p is necessarily between 2 axes k_1 and k_2 of the zone assigned to R. The green circle of radius $d_{\max}$ (the longest axis) represents the first test used to reject a record.*

coordinate system of the current influence zone ($\vec{u}$, $\vec{v}$, $\vec{n}$) is used to determine eight axes around the record position R on its tangent plane. The angle between two successive axes k_i and k_{i+1} is equal to $\frac{\pi}{4}$. An influence zone is then divided into eight subzones, each one being defined by two edges and a pseudo-arc. These two edges have the record position R as an endpoint and are aligned with two successive axes. The lengths of these edges are computed as follows. When computing the irradiance at a record, rays are shot from the record covering an hemisphere placed above it. For each ray close to a footprint axis k_i, we compute the distance to the closest object (called minimum distance from now on) and assign it to the axis. A pseudo-elliptic arc representing the boundary of a subzone is not determined exactly. Rather, it is approximated using a linear interpolation between d_1 and d_2 (the lengths of the edges) if k_1 and k_2 are supposed to be the two successive axes supporting the edges. As described in the Figure 4 , all points P'' lying between k_1 and k_2 on the curved boundary of the surface describe approximately this pseudo-arc:

$$|\overrightarrow{RP''}| = (1-t)\cdot d_1 + t\cdot d_2, \qquad (10)$$

with P' the intersection point between $|\overrightarrow{RP''}|$ and $|\overrightarrow{P_1P_2}|$, $t = |\overrightarrow{P1P'}|/|\overrightarrow{P1P2}|$ and $P_i = R + \overrightarrow{k_i}.d_i$.

To detect if a point p is covered by the influence zone of a record R, we first test if $|x_p - x_R| < d_{k_{\max}}$ with $k_{\max}$ being the longest edge of the eight subzones making up the influence zone. Otherwise, p lies outside the zone. The projection of p onto the tangent plane placed at R is necessarily located between two of the eight axes associated with the record. Then, as seen in Figure 4, it is possible to find P'' using Equation (10). A function similar to the original Ward *et al.* [WRC88] weighting function $w_R(P)$ can be used:

$$w_R(P) = \left(\frac{|\overrightarrow{RP}|}{|\overrightarrow{RP''}|} + \sqrt{1 - \vec{n_p}\cdot\vec{n_R}}\right)^{-1} - 1. \qquad (11)$$

The accuracy parameter a is set to 1 in Equation (11) because the detection of the closest object is more accurate as the length of a footprint axis is a minimum distance. As in the Irradiance Caching method, the record R is rejected if $w_R(P) \leqslant 0$.

In the Cornell Box scene shown in Figure 5, our new record's influence zones are compared to circular zones. Both methods use the minimum distance from close objects and exactly the same criterion (same number of paths for computing irradiance and $a = 1$). Direct contributions are not considered. We observe a large gain in terms of number of records, which results in a smaller computation time because each record requires the same computation time for both methods. As described before, with circular zones, records are concentrated on edges and corners. Adaptive zones better adapt to the geometry and result in a smaller total number of records (see grey scale colour pictures in Figure 5 for the records distribution). The density is lower in the corners and edges for a similar result. However, some artefacts may still exist at the corners because of the ray leaking phenomenon (see [KGW*08]). In what follows, a solution to this issue is

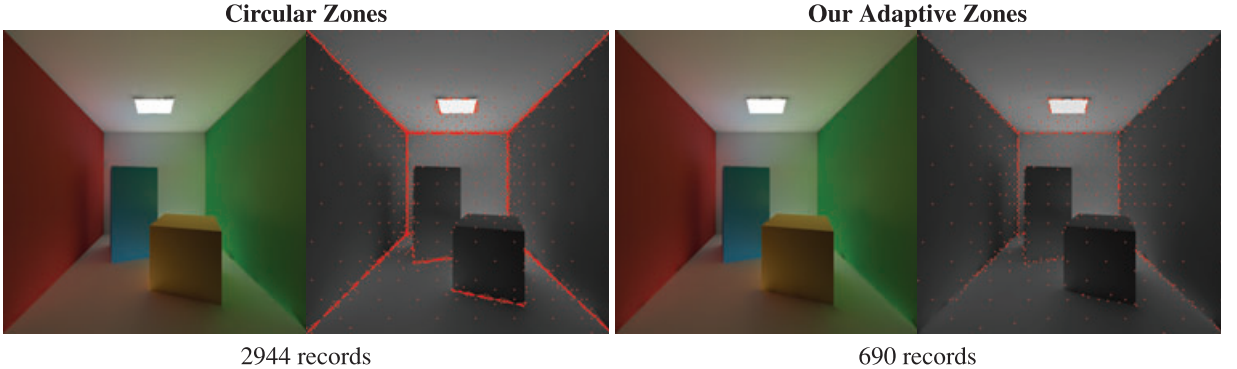

Figure 5: *Circular zones (left panel) and our adaptive zones (right panel) with indirect illumination only; both methods use the minimum distance from close objects and exactly the same criteria. Computation time for one record is the same for both methods. The footprint adjustment depending on the irradiance value (Section 6) has not been performed in this example.*

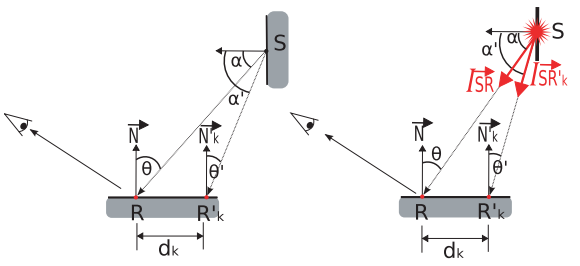

Figure 6: *Two types of equivalent point light source (direct on the right and indirect on the left) are detected for computing irradiance in R. They are used to determine the irradiance at R'_k on the axis k.*

proposed allowing the integration of direct contributions in the records' data structure as well.

5. Gradients Computation

This section presents a novel method of computing translational and rotational gradients for each of the eight record axes. With adaptive record zones, the Ward and Heckbert's gradients [WH92] could be used. As these gradients are of the first order, the irradiance changes are considered as smooth. For high irradiance changes, these gradients are not valid, second-order gradients are then required.

5.1. Computing irradiance along axes

Gradients help determining how the irradiance changes at each point within the record zone. Computing gradients can be achieved by making use of equivalent point light sources described in Section 3 and of Equation (9). The irradiance due to these point light sources can then be computed at every point lying on each axis of the record's influence zone. For point p at position p_x on an axis k of record R, the irradiance is expressed using Equation (12):

$$E(p_x) = \frac{1}{N}\sum_{i=1}^{N} \frac{I_i^{eq}(\overrightarrow{\omega_i}) \cdot (\overrightarrow{n_{p_x}} \cdot \overrightarrow{\omega_i})}{d_i'^2} V(x_i, p_x), \quad (12)$$

where $\overrightarrow{\omega_i}$ is the direction from equivalent point source i to p_x, $I_i^{eq}(\overrightarrow{\omega_i})$ is its equivalent intensity, d_i is the distance between p_x and the equivalent point light source i. $V(x_i, p_x)$ represents the visibility between x_i, the position of the equivalent point light source i, and p_x. $V(x_i, p_x)$ is equal to 1 for an indirect equivalent point light source located at x_i but it is evaluated if x_i belongs to a primary light source. As shown in Figure 6 , two types of contributions are considered: direct and indirect contributions from light sources and objects, respectively. The notations introduced in Figure 6 will be used here (i.e. $\overrightarrow{\omega_i} = \overrightarrow{SR}$ and $\overrightarrow{\omega'_i} = \overrightarrow{SR'_k}$). Let us consider the leftmost figure of Figure 6. It is easy to prove that, for the equivalent point light source S, $I^{eq}(\overrightarrow{SR}) = L(S, \overrightarrow{SR}) \cdot \cos(\alpha)$ and $I^{eq}(\overrightarrow{SR'_k}) = L(S, \overrightarrow{SR'_k}) \cdot \cos(\alpha')$. If we suppose that $L(S, \overrightarrow{SR}) \approx L(S, \overrightarrow{SR'_k})$ then

$$I^{eq}(\overrightarrow{SR'_k}) \approx I^{eq}(\overrightarrow{SR}) \cdot \frac{\cos(\alpha')}{\cos(\alpha)}, \quad (13)$$

where $L(S, \overrightarrow{SR})$ is the radiance at S in direction $\overrightarrow{SR}$, α is the angle between $\overrightarrow{SR}$ and the normal at S.

Let us now consider the rightmost figure of Figure 6 and let S be a point lying on a primary area light source. The intensity at S and for each direction is known (input data). It is easy to prove that $I(\overrightarrow{SR}) = I^{eq}(\overrightarrow{SR}) \cdot \cos(\alpha)$ and $I(\overrightarrow{SR'_k}) = I^{eq}(\overrightarrow{SR'_k}) \cdot \cos(\alpha')$. We get then

$$I^{eq}(\overrightarrow{SR'_k}) = \frac{I(\overrightarrow{SR'_k})}{I(\overrightarrow{SR})} \cdot \frac{\cos(\alpha)}{\cos(\alpha')} \cdot I^{eq}(\overrightarrow{SR}). \quad (14)$$

If we suppose that $\cos(\alpha) \approx \cos(\alpha')$ then we get

$$I^{eq}(\overrightarrow{SR'_k}) \approx I^{eq}(\overrightarrow{SR}) \cdot \frac{I(\overrightarrow{SR'_k})}{I(\overrightarrow{SR})}. \quad (15)$$

Using these two formulations, irradiance can now be computed at each point of each axis.

5.2. Translational gradients

5.2.1. *Computation*

A new method is used to compute gradients to integrate the direct illumination contributions: a second-order Taylor's expansion is introduced for interpolation in the adaptive influence zones. It requires solving an equation expressing the irradiance $\tilde{E}_k(x)$ at a point x on the axis k of the record R:

$$\tilde{E}_k(x) = E(R) + G_k^1 \Delta_k + G_k^2 \frac{\Delta_k^2}{2}, \quad (16)$$

where $\Delta_k = |x - R|_k$ and G_k^1 and G_k^2 are useful interpolation gradients stored in the record and so $\tilde{E}_k(x) = E(x)$. As mentioned earlier, it is possible to know the value of $\tilde{E}_k(x)$ (the irradiance at point x) for all points x on an axis k thanks to Equation (12). If we choose x' at a distance $\Delta' = d_k/2$ from R with d_k the length of the axis k (minimum distance to the closest object along axis k) and x at a distance $\Delta = d_k$, we obtain the following set of equations:

$$\begin{cases} \tilde{E}(x') = E(R) + G_k^1 \Delta' + G_k^2 \Delta'^2/2, \\ \tilde{E}(x) \ = E(R) + G_k^1 \Delta + G_k^2 \Delta^2/2. \end{cases} \quad (17)$$

Applying Equation (12) to express $\tilde{E}(x')$ and $\tilde{E}(x)$ results in a system whose solutions are G_k^1 and G_k^2. The approximated irradiance can now be quickly determined at every point on each axis k of each record using Equation (16).

5.2.2. *Interpolation*

As stated in Section 4, a point P belongs to the influence zone of a record R if its projection onto the tangent plane of R lies within a curved subzone defined by two axes k_1 and k_2 (Figure 4). Equation (16) is expressed for each axis k_n as

$$\tilde{E}_{k_n}(P) = E(R) + G_k^1 \frac{|\overrightarrow{RP}|}{|\overrightarrow{RP''}|} \cdot d_{k_n} + \frac{1}{2} G_k^2 \left(\frac{|\overrightarrow{RP}|}{|\overrightarrow{RP''}|} \cdot d_{k_n} \right)^2 . \quad (18)$$

We assume that the lighting change is linear between two successive axes k_1 and k_2, so the irradiance at P due to R is evaluated using a linear interpolation of the two values $\tilde{E}_{k_1}(P)$ and $\tilde{E}_{k_2}(P)$:

$$E(P) = w_R(P) \cdot \left[\tilde{E}_{k_1}(P) \cdot (1-\tau) + \tau \cdot \tilde{E}_{k_2}(P) \right], \quad (19)$$

where after Thales theorem $\tau = |\overrightarrow{P_1P'}|/|\overrightarrow{P_1P_2}|$. We define $Tr(P) = \left[\tilde{E}_{k_1}(P) \cdot (1-\tau) + \tau \cdot \tilde{E}_{k_2}(P) \right]$ as the translational term for the point P. The above assumption provides good results in practice.

5.3. Rotational gradients

5.3.1. *Computation*

Rotational gradients help determining the irradiance variation due to normal perturbation. A new method of rotational gradient computation is proposed in this section. Our approach computes eight rotational gradients, each corresponding to a normal perturbation of maximum angle $\alpha_{\max}$ along one axis associated with the influence zone of a record. Using Equation (7), irradiance can be computed for a normal vector $\overrightarrow{n'_k}$, a perturbation of the normal vector $\overrightarrow{n_R}$ of the record R along the axis k:

$$E(\overrightarrow{n'_k}) = \frac{1}{N} \sum_{i, (\overrightarrow{n'_k} \cdot \overrightarrow{\omega_i}) > 0}^{N} \frac{I_i^{\text{eq}}(\overrightarrow{\omega_i}) \cdot (\overrightarrow{n'_k} \cdot \overrightarrow{\omega_i})}{d_i^2}. \quad (20)$$

A second-order Taylor expansion is a function of Δ_θ, the angular distance between the normal vector $\overrightarrow{n_R}$ of the record R, and $\overrightarrow{n'_k}$, the perturbed normal vector by an angle $\alpha_{\max}$:

$$\tilde{E}(\alpha_{\max}) = E(R) + G_k^{\text{rot1}} \Delta_\theta + \frac{1}{2} G_k^{\text{rot2}} \Delta_\theta^2. \quad (21)$$

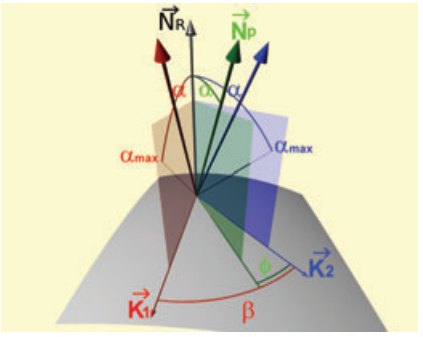

Figure 7: *Rotational interpolation. ϕ is the angle between the $(\vec{N}_R, \vec{N}_P)$ and the $(\vec{k}_2, \vec{N}_R)$ planes.*

Similarly to translational gradients and Equation (17), we get

$$\begin{cases} E\left(\frac{\alpha_{\max}}{2}\right) = E(R) + G_k^{\text{rot1}} \frac{\Delta_\theta}{2} + \frac{1}{2} G_k^{\text{rot2}} \left(\frac{\Delta_\theta}{2}\right)^2, \\ E(\alpha_{\max}) = E(R) + G_k^{\text{rot1}} \Delta_\theta + \frac{1}{2} G_k^{\text{rot2}} (\Delta_\theta)^2. \end{cases} \quad (22)$$

5.3.2. *Interpolation*

As in the case of translation interpolation, when a point P lies within the influence zone of the record R, then its orthogonal projection onto the tangent plane of R lies necessarily between two successive axes. Let us suppose that these axes are $\overrightarrow{k_1}$ and $\overrightarrow{k_2}$. The normal vector $\overrightarrow{n_P}$ at P also ranges between two normal perturbation vectors on each axis (Figure 7). As in the case of translation interpolation, we make the same empirical assumption regarding irradiance changes: we consider them as linear between two successive axes. The rotational term $Rot(P)$ may be written as

$$\text{Rot}(P) = \left[\frac{\phi}{\beta} \cdot \tilde{E}_{k_1}(\alpha) + \left(1 - \frac{\phi}{\beta}\right) \cdot \tilde{E}_{k_2}(\alpha) \right], \quad (23)$$

where ϕ is the angle between the projection plane of normal $\overrightarrow{n_R}$ and $\overrightarrow{k_2}$, and $\beta = \pi/4$ is the angle between $\overrightarrow{k_1}$ and $\overrightarrow{k_2}$ (Figure 7). The interpolation of irradiance at a point P within the influence zone of the record R using rotational gradients is expressed as

$$E(P) = w_R(P) \cdot (\text{Tr}(P) + \text{Rot}(P)). \quad (24)$$

Doing a slight modification of the weighting function which must tend towards 0 when α tends towards $\alpha_{\max}$ to avoid a discontinuity at the border of the influence area (see [KGW*08] and Section 3), we get

$$w_R(P) = \left(\frac{|\overrightarrow{RP'}|}{|\overrightarrow{RP}|} - 1 \right) \cdot \left(1 - \frac{\alpha}{\alpha_{\max}} \right) \quad (25)$$

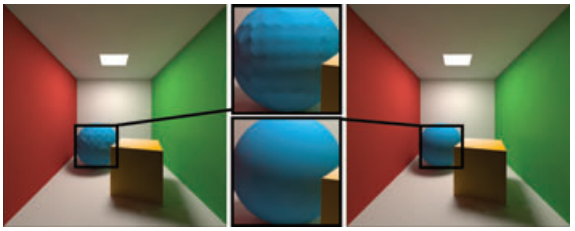

Figure 8: *Ward and Heckbert's rotational gradients (left) and our rotational gradients (right) with direct and indirect illumination; both methods give the same number of records (around 150 records on the sphere). In our gradients,* $\alpha_{\max}$ *is fixed to* 20°

In fact, we replace Equation (11) by Equation (25) because we allow a rotational perturbation of an angle α ranging between 0 and $\alpha_{\max}$ and assume that the weights vary linearly with the angle α.

Figure 8 shows an example where Ward and Heckbert's rotational gradients are not accurate enough when direct contributions are stored in the records. Both methods use adaptive records described in Section 4 as well as translational gradients described in the previous section. Our rotational gradients provide smoother results on curved surfaces.

6. Size of Zones Based on Interpolation Accuracy

Storing direct lighting into records saves a lot of time in case of complex lighting conditions. However, despite the quadratic gradients interpolation, some lighting situations, such as the presence of shadows, can be sources of artefacts. To cope with these cases, it is possible to adjust the size of a record's influence zone depending on the irradiance change over this zone. The higher the irradiance change along an axis k_i of the zone, the smaller the length of this axis. In this paper, the interpolation quality is controlled during the computation of a record (Figure 9). Ray tracing is used to compute the irradiance of a record R together with its initial length axes (size of the influence zone for each axis on the tangent plane associated with R). For each axis k_i, the translational gradients are computed at a point R' at a distance d_i (the initial length of the axis k_i) from R and at a point R'' at distance $d_i/2$. Two other intermediate points are used: R_1 at distance $d_i/4$ and R_2 at distance $3d_i/4$. These two points are assigned two different values: one computed using Equation (12) [$E(R_1)$ and $E(R_2)$], the other [$\tilde{E}(R_1)$ and $\tilde{E}(R_2)$] interpolated using Equation (16) where x is equal to R_1 or R_2 and Δ_k to $\|RR_1\|$ or $\|RR_2\|$, respectively. If the error $\frac{E(R_1)-\tilde{E}(R_1)}{E(R_1)}$ [or $\frac{E(R_2)-\tilde{E}(R_2)}{E(R_2)}$ for point R_2] exceeds a threshold ρ set by the user, then the interpolation quality is not satisfactory. In this case, the process proceeds as follows. First, we reduce the distance d_i to $\|RR_2\|$. Secondly, to save computation time, the new R' replaces the previous R_2, the new R_2 replaces the previous R'' and R_1 does not change. Consequently, the irradiance values at the new points R', R_2 and R_1 are not recomputed, only the new R'' (middle of the segment whose endpoints are R and the new R') as well as its irradiance have to be recomputed. This technique has the effect of increasing the concentration of records in areas where irradiance gradients are not valid for interpolation purpose.

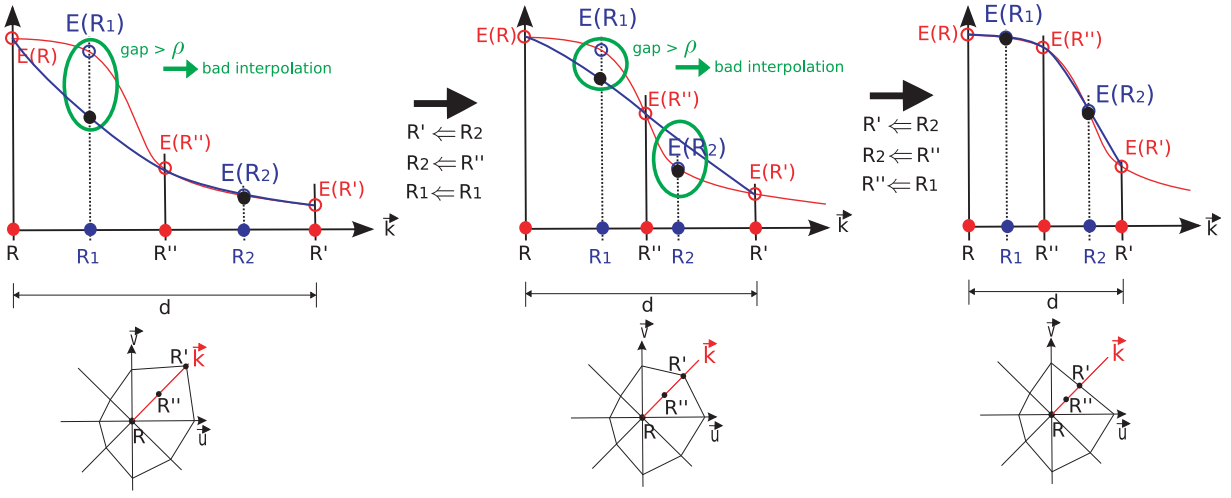

Figure 9: *Points* R' *and* R'' *together with the intermediate points* (R_1 *and* R_2) *are used to determine if irradiance interpolation (the blue curve) is accurate. Interpolation is inaccurate if the relative difference between* $\tilde{E}(R_1)$ *and* $\tilde{E}(R_2)$ *[computed using Equation (16) at points* R_1 *and* R_2 *represented by black dots] and the actual values* $E(R_1)$ *and* $E(R_2)$ *[computed using Equation (12), represented by blues circles] exceeds the threshold* ρ *fixed by user. See Section 6 for more details.*

7. Results and Discussion

7.1. General comments on results

In physics-based lighting design, light/material interaction must be simulated as accurately as possible. Results must of course be consistent with the physical reality. All results presented in this paper are obtained without any restriction on the number of indirect bounces. The physical quantities, radiance and irradiance, are represented by spectra of 40 wavelengths. The light sources and their photometric features are defined by *IES* (Illuminating Engineering Society of North America) and stored in specific files (see standard [IES02]).

The *Adaptive Records for Irradiance Caching* method presented in this paper (called *ARIC* from now on) has been compared with several other techniques. The classical BPT (*Bidirectional Path Tracing* [VG94, Vea98] and [LW93]) was first considered. Then, two versions of the Irradiance Caching algorithm have been used. A first method (called *MDIC*) relies on circular zones and uses a minimum distance for computing the weighting coefficients. A second method (called *HMDIC*) uses circular influence zones, harmonic mean distance (rather than minimum distance), *neighbour clamping* and the *adaptive caching* test proposed in [KBPv06]. It is of course possible to include these optimizations in our method. Nevertheless, the results presented in this section have been obtained without this optimization. For all the other Irradiance Caching methods, direct illumination is not stored in the records, rather it is recomputed in the rendering pass.

All the methods that are compared to ours are integrated into a same renderer. Results have been obtained on an Intel Core 2 Q9550 (2.83 GHz) with 4 GByte of RAM (using a single core) running on a 64 bits version of linux operating system.

7.2. Cornell box scene results

Figure 10 shows renderings of the well-known Cornell Box scene with the four above-mentioned methods. The rendering resolution is 800×800 pixels. Rendering statistics are given in Table 1. BPT has been calibrated to take approximately the same time as our new method (12 samples per pixel). The Irradiance Caching methods have been run with the objective of providing the same perceptive results. To evaluate irradiance similar convergence criteria for Monte Carlo sampling are used for all methods. Direct contributions are recomputed for all pixels (for the *MDIC* and *HMDIC* methods), 30 shadow rays are cast to sample the area light source. Parameter a is set to 0.4 for the *HMDIC* method while it is equal to 1 for the *MDIC* method. Note that with the *ARIC* method, the records are concentrated around the shadow to better capture the abrupt illumination changes. For the same image quality, our adaptive approach outperforms the other methods in terms of rendering time.

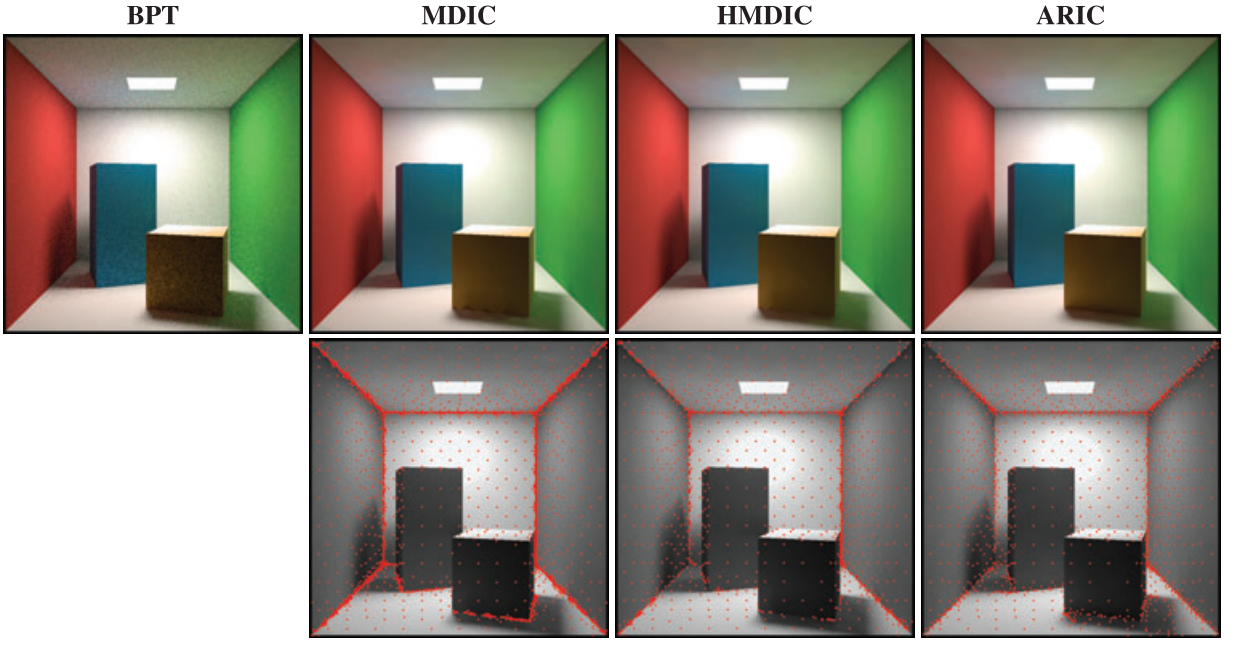

Figure 10: *Four views of the Cornell Box scene rendered with four different methods. With our adaptive records method (on the right), the record density is higher in areas of high gradients (here along the shadow edges).*

Table 1: *Rendering statistics for the Cornell Box scene: cache filling is the time (expressed in seconds) spent for creating records and storing them in the cache.*

	No. of records created	Cache filling	Rendering pass	Total time
BPT	–	–	81	81
MDIC	2798	200	47	247
HMDIC	1443	102	47	149
ARIC	**1371**	**74**	**6**	**80**

Note: Rendering pass is the time spent for creating the final pictures (interpolation from the cached records and evaluation of the direct contributions for the *MDIC* and *HMDIC* methods). BPT needs only a Rendering Pass.

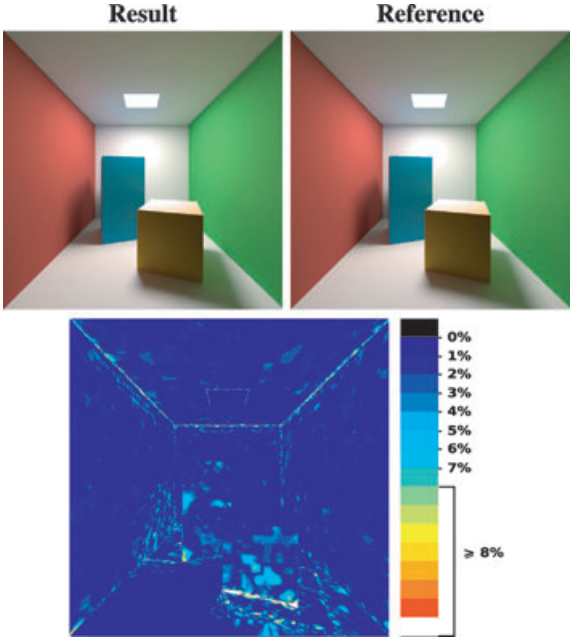

Figure 11: *Relative difference between the image calculated with our method and a reference picture: the mean relative difference is* 1%.

Figure 11 shows the difference between an image generated with our method and a reference image. The image with a 800×800 pixel resolution is computed with 1300 records. The average relative difference on all non-zero points is 1%. Most errors are located on the edges of the shadows: a smaller threshold ρ_{mini} could solve the problem. Other errors located on surfaces can be corrected by a better Monte Carlo sampling.

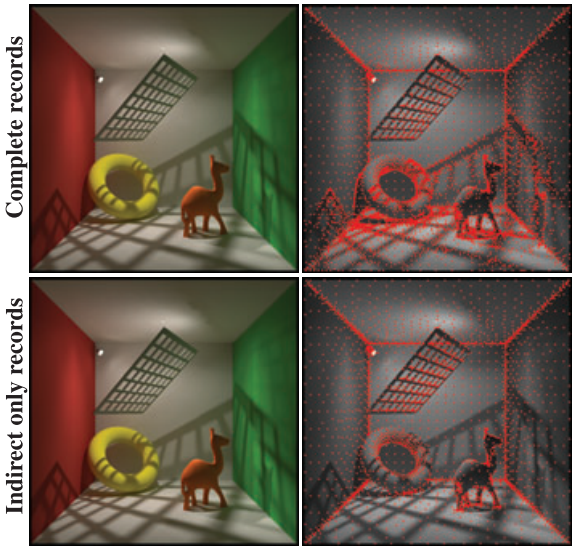

Figure 12: *Scene composed of curved surfaces and exhibiting high-frequency illumination. The first row is computed with adaptive records storing direct and indirect illuminations while the second row with adaptive records storing only indirect illumination (direct illumination is recomputed in a rendering pass). The images in the second row are of better quality but require twice the computation time.*

7.3. Llama, torus and grid scene results

The scene (Llama, torus and grid) shown in Figure 12 is composed of curved surfaces and exhibits high-frequency illumination. High-frequency illumination due to small area light sources is difficult to compute with Irradiance Caching because some effects can be missed. Monte Carlo sampling seems to be better because few shadow rays are needed to capture direct illumination. Storing direct illumination in the records could be less interesting for this kind of scene. Figure 12 compares two version of our *ARIC* : (1) direct and indirect illuminations are stored in the records, (2) only indirect contributions are stored. The same parameters are used for both versions. The direct contributions are recomputed for version 2. As our method adapts the cache density in regions of high illumination change, the results of Figure 12 show two different records distributions for the two versions. For version 1, the records are concentrated around shadow edges. In this example, more records are needed for version 1 (6016 records) than for version 2 (3241 records) because of the high-frequency illumination changes. However, version 1 takes twice less time than version 2 for exactly the same parameters. Consequently, version 1 of our method performs well in case of strong indirect or direct illumination changes.

Figure 13 shows the impact of the threshold ρ on a close-up view of the scene shown in Figure 12 and computed with our *ARIC* method where the records store direct and

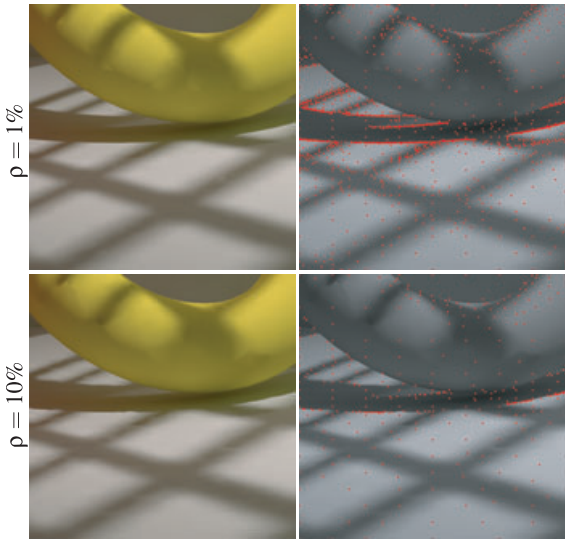

Figure 13: *Impact of the threshold ρ on the quality of the high-frequency illumination effects and on the records density.*

indirect illuminations. Both results are computed with the same parameters, only the threshold ρ is different. A restrictive threshold (e.g. 1%) allows to concentrate records density around strong illumination gradients while a permissive threshold (e.g. 10%) can miss this kind of effects. In case of complete records with a low threshold in a scene composed of high-frequency illumination, interpolation artefacts appear around shadow edges. A restrictive threshold solves the problem by adding records around high frequency illumination effects.

7.4. Villa Arpel scene results

Figure 14 shows two close-up views of the villa Arpel scene generated with our method and the two other Irradiance Caching methods. The image in Figure 15 represents the complete villa Arpel scene generated with our method. The images resolutions are 800 × 800 pixels for the close-up views and 1920 × 1080 pixels (full high definition) for Figure 15. The rendering results are given in Table 2 for the two close-up views. The results have been obtained with complex

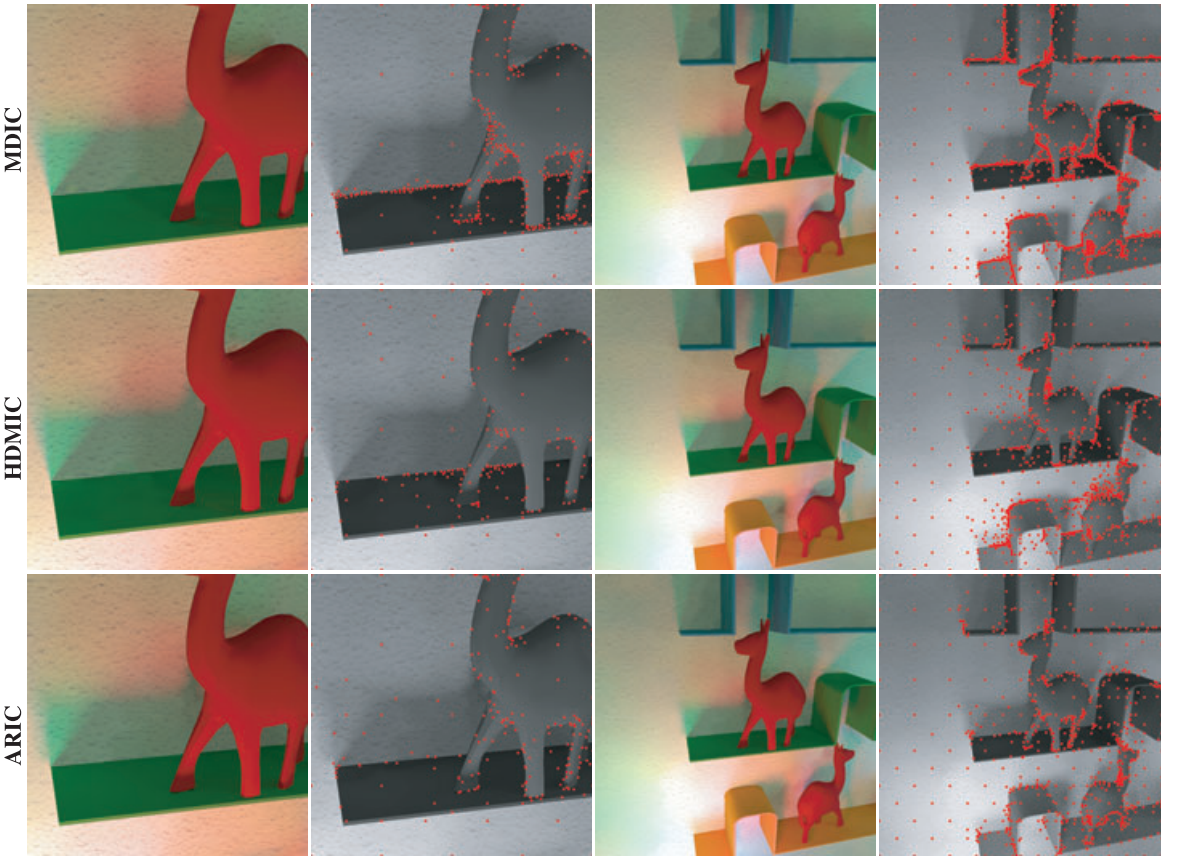

Figure 14: *Two close-up views of the villa Arpel scene rendered with different methods. The cached points are represented in red colour.*

Figure 15: *Villa Arpel scene rendered with our adaptive records method.*

Table 2: *Rendering statistics for results seen in Figure 14.*

		No. of records created	Cache filling	Total time
First close-up	*MDIC*	380	7 min 59 s	2 h 47 min
	HMDIC	197	3 min 3 s	2 h 40 min 30 s
	ARIC	**209**	**3 min 10 s**	**3 min 16 s**
Second close-up	*MDIC*	1247	18 min 15 s	2 h 34 min 6 s
	HMDIC	798	12 min 9 s	2 h 56 min 24 s
	ARIC	**523**	**6 min 50 s**	**6 min 57 s**

artificial lighting conditions (11 light sources made up of 760 polygons with different coloured spectra) and overcast sky for daylighting conditions obtained with a standard CIE sky model (see CIE standards in [CIE96]). Given the high number of light sources, it is particularly interesting to store direct contributions in records to save computation time. All the methods have the same parameters. Direct contributions are computed using 4000 shadow rays for all the artificial light sources. Parameter a is set to 0.4 for the *HMDIC* method and 1 for the methods using a minimum distance. The image in Figure 15 has been computed in 1 h and 6 min (and 33 s for the rendering pass) with 6962 cached points, whereas the *HMDIC* method took 1 h and 30 min (and 8 h for the rendering pass) with 6656 records. As shown in Figure 14, our method provides a better record distribution while reducing the total number of records. In addition, for the same image quality, our ARIC method outperforms the other methods.

8. Conclusion

We have presented a new method to adaptively compute records in an Irradiance Caching algorithm. We have proposed a new record footprint specifically built to account for both geometrical and irradiance changes over surfaces. Our approach prevents the cache from being too dense at the edges and borders of the scene's objects. Including irradiance changes in the translational gradient computations leads to a denser cache in areas subject to large irradiance changes. It thus compensates for any inaccurate interpolation appearing with complex changes of irradiance. Such a feature allowed us to successfully store direct illumination in the records and to significantly speed up the rendering pass. The storage of the direct irradiance is interesting especially in the case of complex lighting conditions such as combined daylighting and artificial lighting. Similarly, large area light sources or animation rendering could also benefit from this characteristic because direct lighting does not have to be computed for successive frames but rather interpolated.

In a future work, the Radiance Caching scheme will be investigated to include in the adaptive record method more directional information such as glossy reflection.

Acknowledgments

This work has been carried out with the financial support of ANRT within the framework of the CSTB Institut Carnot 2009 research program. Thanks go to Luis Paulo dos Santos for his helpful comments on the paper.

References

[BWG03] Bala K., Walter B., Greenberg D. P.: Combining edges and points for interactive high-quality rendering. *ACM Transactions on Graphics 22*, 3 (2003), 631–640.

[CIE96] CIE: Spatial distribution of daylight - cie standard overcast sky and clear sky. In *Proceedings of CIE S 003/E-1996* (Vienna, Australia, 1996).

[GKPB04] Gautron P., Křivánek J., Pattanaik S. N., Bouatouch K.: A novel hemispherical basis for accurate and efficient rendering. In *Proceedings of Rendering Techniques 2004, Eurographics Symposium on Rendering* (Norrköping, Sweden, June 2004), pp. 321–330.

[Gre03] Green R.: Spherical harmonic lighting: The gritty details. In *Proceedings of Archives of the Game Developers Conference* (San Jose, CA, USA, March 2003).

[HMS09] Herzog R., Myszkowski K., Seidel H.-P.: Anisotropic radiance-cache splatting for efficiently computing high-quality global illumination with lightcuts. In *Computer Graphics Forum (Proc. EUROGRAPHICS)* (München, Germany, 2009), M. Stamminger, P. Dutré (Eds.), vol. 28, Wiley-Blackwell, Oxford, pp. 259–268.

[IES02] IESNA: Iesna standard file format for the electronic transfer of photometric data and related information. In *LM-63-02* (September 2002), IESNA, New York, NY.

[KBPv06] Křivánek J., Bouatouch K., Pattanaik S. N., Žára J.: Making radiance and irradiance caching practical: Adaptive caching and neighbor clamping. In *Proceedings of Rendering Techniques 2006, Eurographics Symposium on Rendering* (Nicosia, Cyprus, June 2006), T. Akenine-Möller, W. Heidrich (Eds.), Eurographics Association, Eurographics Association.

[KGBP05] Křivánek J., Gautron P., Bouatouch K., Pattanaik S.: Improved radiance gradient computation. In *SCCG'05: Proceedings of the 21st Spring Conference on Computer Graphics* (New York, NY, USA, 2005), ACM Press, pp. 155–159.

[KGPB05] Křivánek J., Gautron P., Pattanaik S., Bouatouch K.: Radiance caching for efficient global illumination computation. *IEEE Transactions on Visualization and Computer Graphics 11*, 5 (September/October 2005), 550–561. http://graphics.cs.ucf.edu /RCache/index.php.

[KGW*08] Křivánek J., Gautron P., Ward G., Jensen H. W., Tabellion E., Christensen P. H.: Practical global illumination with irradiance caching. In *Proceedings of ACM SIGGRAPH '08 Class* (Los Angeles, CA, USA, 2008). http://www.graphics.cornell.edu/ jaroslav/papers/2008-irradiance_cachin g_class/index.htm.

[Kŭ05] Křivánek J.: *Radiance Caching for Global Illumination Computation on Glossy Surfaces*. PhD thesis, Université de Rennes 1 and Czech Technical University in Prague, December 2005.

[LW93] Lafortune E. P., Willems Y. D.: Bi-directional path tracing. In *Proceedings of Third International Conference on Computational Graphics and Visualization Techniques (Compugraphics '93)* (Alvor, Portugal, 1993), H. P. Santo (Ed.), pp. 145–153.

[RFT06] Robert F., Tobler S. M.: Improved illumination estimation for photon maps in architectural scenes. In *Proceedings of WSCG (International Conference in Central Europe on Computer Graphics, Visualization and Computer Vision)* (Plzen, Czech Republic, 2006), pp. 257–262.

[SM02] Smyk M., Myszkowski K.: Quality improvements for indirect illumination interpolation. In *Proceedings of the International Conference on Computer Vision and Graphics* (Zakopane, Poland, 2002).

[TL04] Tabellion E., Lamorlette A.: An approximate global illumination system for computer generated films. In *Proceedings of SIGGRAPH '04: ACM SIGGRAPH 2004 Papers* (New York, NY, USA, 2004), ACM, pp. 469–476.

[VALBW06] Velázquez-Armendáriz E., Lee E., Bala K., Walter B.: Implementing the render cache and the edge-and-point image on graphics hardware. In *GI '06: Proceedings of the 2006 Conference on Graphics Interface* (Toronto, Ont., Canada, Canada, 2006), Canadian Information Processing Society, pp. 211–217.

[Vea98] Veach E.: *Robust Monte Carlo Methods for Light Transport Simulation*. PhD thesis, Stanford University, Stanford, CA, USA, 1998. Adviser-Leonidas J. Guibas.

[VG94] Veach E., Guibas L. J.: Bidirectional estimators for light transport. In *Proceedings of the Eurographics Rendering Workshop* (Darmstadt, Germany, June 1994), Springer-Verlag, New York, pp. 147–162.

[WABG06] Walter B., Arbree A., Bala K., Greenberg D. P.: Multidimensional lightcuts. In *Proceedings of the SIGGRAPH '06: ACM SIGGRAPH 2006 Papers* (New York, NY, USA, 2006), ACM, pp. 1081–1088.

[WDG02] Walter B., Drettakis G., Greenberg D.: Enhancing and optimizing the render cache. In *Proceedings of the Eurographics Workshop on Rendering*, P. Debevec, S. Gibson (Eds.), Eurographics, ACM Press, Pisa, Italy (June 2002).

[WDP99] Walter B., Drettakis G., Parker S.: Interactive rendering using the render cache. In *Rendering*

Techniques (Proceedings of the Eurographics Workshop on Rendering) (New York, NY, June 1999), D. Lischinski, G. Larson (Eds.), vol. 10, Springer-Verlag/Wien, pp. 235–246.

[WFA*05] Walter B., Fernandez S., Arbree A., Bala K., Donikian M., Greenberg D. P.: Lightcuts: A scalable approach to illumination. *ACM Transactions on Graphics 24*, 3 (2005), 1098–1107.

[WH92] Ward G., Heckbert P.: Irradiance gradients. In *Proceedings of the Eurographics Rendering Workshop* (Bristol, UK, May 1992), pp. 85–98.

[WRC88] Ward G. J., Rubinstein F. M., Clear R. D.: A ray tracing solution for diffuse interreflection. In *SIGGRAPH '88: Proceedings of the 15th Annual Conference on Computer Graphics and Interactive Techniques* (New York, NY, USA, 1988), ACM, pp. 85–92.